

Production and rescattering of strange baryons at SPS energies in a transport model with hadron potentials

Qingfeng Li,^{1*} and Zhuxia Li²

1) School of Science,

Huzhou Teachers College,

Huzhou 313000, P.R. China

2) China Institute of Atomic Energy,

P.O. Box 275 (18),

Beijing 102413, P.R. China

Abstract

A mean-field potential version of the Ultra-relativistic Quantum Molecular Dynamics (UrQMD) model is used to investigate the production of strange baryons, especially the Λ s and $\bar{\Lambda}$ s, from heavy ion collisions at SPS energies. It is found that, with the consideration of both formed and pre-formed hadron potentials in UrQMD, the transverse mass and longitudinal rapidity distributions of experimental data of both Λ s and $\bar{\Lambda}$ s can be quantitatively explained fairly well. Our investigation also shows that both the production mechanism and the rescattering process of hadrons play important roles in the final yield of strange baryons.

PACS numbers: 25.75.Gz,25.75.Dw,24.10.Lx

* E-mail address: liqf@hutc.zj.cn

The heavy ion collision (HIC) is the only way of the human being at present to explore the properties of nuclear matter at supranormal and subnormal densities and/or high temperatures. The properties of the sub-structure and the dynamics of the nucleus/nucleon could be even discovered by high-energy HICs which has being explored experimentally by the SchwerIonen Synchrotron (SIS) at Gesellschaft für Schwerionenforschung (GSI, Germany), the Alternating Gradient Synchrotron (AGS) at the Brookhaven National Laboratory (BNL,USA), the Super Proton Synchrotron (SPS) at the European Organization for Nuclear Research (CERN, Switzerland), the Relativistic Heavy Ion Collider (RHIC) at BNL, and the Large Hadron Collider (LHC) at CERN. Theoretically, the most important property of the nuclear matter relates closely to its equation of state (EoS) [1–4]. The stiffness of the EoS at both low and high densities have also being received much attention in past decades [5–11]. At high densities, the stiffness of the EoS will definitely decide the order and the level of the phase transition to the quark-gluon plasma (QGP) [12–16]. It is a consensus that any final conclusion of it should only be drawn by large numbers of comparison works between theoretical simulations and experimental measurements.

In the past, several signals - such as charmonium suppression, relative strangeness enhancement, energy loss of hard partons, etc - of the (phase) transition to the deconfined phase have been observed in HICs at SPS energies [17–22]. However, none of them gives 100% undoubt conclusion of the probable phase transition. Especially, the strangeness production and enhancement is still a matter of argument. It is quite necessary to investigate the strange hadrons with a microscopic transport model which might give deeper insights into the whole process of the production and the transport of all hadrons. The Ultra-relativistic Quantum Molecular Dynamics (UrQMD) [15, 23–26] is one of the most suitable microscopic transport models which have been worked fairly successfully in this field for more than 10 years in addition to the Relativistic Quantum Molecular Dynamics (RQMD) [27], the Parton-Hadron-String Dynamics (PHSD) [28] and A MultiPhase Transport model (AMPT) [29] models.

However, based on previous comparison of UrQMD calculations with data, we know that there are some disagreement about the strange hadron production at AGS and SPS energies [23, 30, 31]. As for hyperons, first, the yields of hyperons are somewhat overestimated in UrQMD cascade calculations using versions earlier than 2.1. Starting from version 2.1, the UrQMD group considers additional high mass resonances which leads to a smaller yield of

hyperons so that a nice agreement with data from central Pb+Pb collisions at SPS energies was seen in previous calculations [25]. Second, the resulting mean transverse momenta of hyperons were found to be too low as compared with experimental data when using the version earlier than 2.1 [31]. It is interesting to see that this problem is also partly cured by the newest version 2.3. Third, even though the former two problems have been cured partly with the updating cascade version, the yield of anti-hyperons decreases at the same time which makes the comparison with data become even worse [31]. These problems attract our attention and will be discussed in this paper with a mean-field potential version of the UrQMD model.

In this paper, after a brief introduction of the UrQMD and its recent updates, the production and the evolution of strange hadrons as well as anti-protons at SPS energies are investigated with the mean-field potential version. For comparison, the corresponding cascade calculation results are also shown. The experimental data are taken from NA49 collaboration [32–34]. Finally, a conclusion and outlook is given.

The UrQMD model is a microscopic transport approach based on the covariant propagation of constituent (anti-)quarks and diquarks accompanied by mesons and baryons, as well as the corresponding anti-particles, i.e., full baryon-anti-baryon symmetry is included. It simulates multiple interactions of ingoing and newly produced particles, the excitation and fragmentation of color strings and the formation and decay of hadronic resonances [23, 24]. Besides the cascade mode in which all particles are treated to be free streaming between collisions, it is also necessary to incorporate the mean-field contribution for a complete dynamic transport [15, 35, 36]. Since the UrQMD model inherits the basic treatment of the baryonic equation of motion in the QMD model [37], the consideration of the mean-field contribution is also logical. In order to properly describe the physical process in HICs at SIS energies this term has been treated carefully in the UrQMD model before [38–40]. With the increase of beam energy from SIS, AGS, SPS, up to RHIC, the dynamics of the transport has being attracted more and more attention due to the fact that quite a few of discrepancies between cascade calculations, of any microscopic transport models, and experimental data have been shown in these beam energy regions, such as the collective flows [38, 41], the nuclear stopping [25, 40], and the HBT two-particle correlation [36, 42].

Recent update of the UrQMD model follows three different routines. The first one is called as “cascade version” which is to modify the cascade process of UrQMD. This is the main

routine and the newest official version is v2.3 [31]. The second one is called as “mean-field potential version” which further considers the mean-field potentials of both formed and pre-formed hadrons [36]. The third one is called as “hybrid version” with which the microscopic transport process is incorporated with a macroscopic hydrodynamics [15, 43]. So, by using the ‘hybrid version’ one can compare calculations with various EoS during the hydrodynamic evolution and those with the pure cascade calculations within the same framework. The first routine is of importance since it supplies a better basis as a cascade process. The latter two versions consider more deeply about the dynamic process of all particles but with different strategies: The second routine bases on the same structure of the equation of motion at low SIS beam energies, in which both the mean field and the collision terms should be taken into account explicitly. While the third routine replaces the UrQMD dynamic process in between the initialization and the hadron rescattering processes by a hydrodynamic one. Therefore, one sees clearly that, with the rapid development of researches on the dynamic process of high-energy HICs, the modifications on the transport model are still quite frequent and effective.

Starting from the version 2.0, similar to HSD, the PYTHIA [44] is considered in order to treat the initial hard collisions more carefully, which is important for HICs at high SPS and RHIC energies. In the version 2.1 [25], similar to RQMD, the high-mass resonances are re-treated in order to give higher mean transverse momenta of most particles. The newest version 2.3 [31] is then brought out with some other minor changes. The mean-field potential version is based on the cascade version v2.1 but not v2.3 which is partly due to the minor difference between them. As for the mean-field contribution, in addition to the conventional potentials for formed hadrons [35], the mean-field potentials for pre-formed baryons from string fragmentation have also been taken into account [36], i.e., the Yukawa, the Coulomb, and the momentum dependent terms are neglected but the similar density dependent (Skyrme-like) term as the formed baryons is used, which reads as

$$U(\rho_h/\rho_0) = a\left(\frac{\rho_h}{\rho_0}\right) + b\left(\frac{\rho_h}{\rho_0}\right)^g, \quad (1)$$

while a reduction factor (2/3) is considered for pre-formed mesons due to the quark-number difference. In Eq. (1) $\rho_0 = 0.16 fm^{-3}$ is the normal nuclear density. a , b , and g are parameters, in this work for the SM-EoS, they are -110 MeV, 182 MeV, and $7/6$, respectively. The ρ_h is the hadronic density, which reads as

$$\rho_h = \sum_{j \neq i} c_i c_j \rho_{ij} \quad (2)$$

where $c_{i,j} = 1$ for baryons, $2/3$ for pre-formed mesons, and 0 for formed mesons. ρ_{ij} is a Gaussian in coordinate space.

As in Ref. [45], the relativistic effects on the relative distance $\mathbf{r}_{ij} = \mathbf{r}_i - \mathbf{r}_j$ and the relative momentum $\mathbf{p}_{ij} = \mathbf{p}_i - \mathbf{p}_j$ employed in the two-body potentials (Lorentz transformation) are considered as follows:

$$\tilde{\mathbf{r}}_{ij}^2 = \mathbf{r}_{ij}^2 + \gamma_{ij}^2 (\mathbf{r}_{ij} \cdot \beta_{ij})^2, \quad (3)$$

$$\tilde{\mathbf{p}}_{ij}^2 = \mathbf{p}_{ij}^2 - (E_i - E_j)^2 + \gamma_{ij}^2 \left(\frac{m_i^2 - m_j^2}{E_i + E_j} \right)^2. \quad (4)$$

In Eqs. 3 and 4 the velocity factor β_{ij} and the corresponding γ -factor of i and j particles are defined as $\beta_{ij} = (\mathbf{p}_i + \mathbf{p}_j)/(E_i + E_j)$ and $\gamma_{ij} = 1/\sqrt{1 - \beta_{ij}^2}$. Furthermore, a covariance-related reduction factor for potentials in the Hamiltonian, m_j/E_j , was introduced in the simplified version of RQMD model [46] and adopted in this work as well.

We have found from the HBT correlations of two-particles at AGS, SPS, and RHIC energies that the mean-field potentials of both formed and pre-formed hadrons are essential for explaining the sources of the HBT time-related puzzle [36, 47]. Furthermore, by using the hybrid model, it is found that the equation of state at high densities should be somewhat stiff in order to explain the HBT data at SPS energies [15]. Although, the stiffness of the EoS is still with some uncertainties, it is no doubt that the dynamic process deserves more investigations. We notice that the average hadronic density at a central zone (e.g., $R_{c.m.} < 5fm$) from central Pb+Pb reactions at SPS energies reaches 4-8 times normal nuclear density at the early stage of the collision. And, it is known that in the same beam energy region and at the early stage, the string process starts to replace the resonance-decay process for producing new particles in the UrQMD model description. Fig. 1 shows the time evolution of the ratio of pre-formed hadrons and all hadrons (“ $R_{pre-formed/all}$ ”) in the zone $R_{c.m.} < 5fm$ from the central Pb+Pb reaction at 40A GeV (solid line) and 158A GeV (dashed line), respectively. It is seen clearly that the main production mechanism at $t < 5$ fm/c is the string excitation and fragmentation. And it is up to $t \sim 10$ fm/c that this production mechanism still plays visible role. Hence, the pre-formed hadron potentials will definitely provide a large contribution to the early pressure. Accordingly, the rescattering

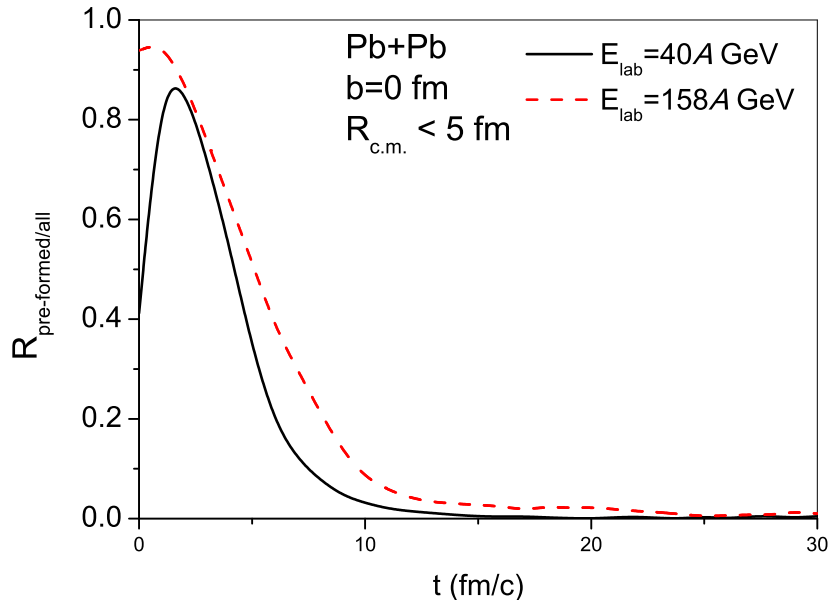


FIG. 1: Time evolution of the ratio of pre-formed hadrons and all hadrons (“ $R_{pre-formed/all}$ ”) in the zone $R_{c.m.} < 5 fm$ from central Pb+Pb reaction at 40A GeV (solid line) and 158A GeV (dashed line), respectively.

of new produced particles will be influenced to some extent, which will be checked by the current investigation.

Fig. 2 shows the transverse mass ($m_t - m_0$, where $m_t = \sqrt{p_t^2 + m_0^2}$ and m_0 is the mass of the particle at rest, $p_t = \sqrt{p_x^2 + p_y^2}$ is the transverse momentum of the particle in the center-of-mass system) spectra of Λ_s ($= \Lambda + \Sigma^0$, same as experimental data) at mid-rapidity ($|y| < 0.4$) for central Pb+Pb reactions ($\sigma/\sigma_T < 5\%$) at 40A GeV (left plot) and at 158A GeV (right plot). The data are taken from Ref. [34] for comparison. We find that the cascade calculation of the UrQMD version 2.1 already reproduces the data well within error bars except those at very low and high transverse masses. We also noticed that if the newest version 2.3 is used this situation becomes even worse at large transverse masses, which might be due to the minor changes of the double strange diquark suppression factor and the single strange diquark suppression factor. If we use the older version 1.3, as we have known before [31], the slope of the transverse mass spectra is steeper than the newest one. Hence the careful treatment of the high-mass resonances is very important. With the consideration of

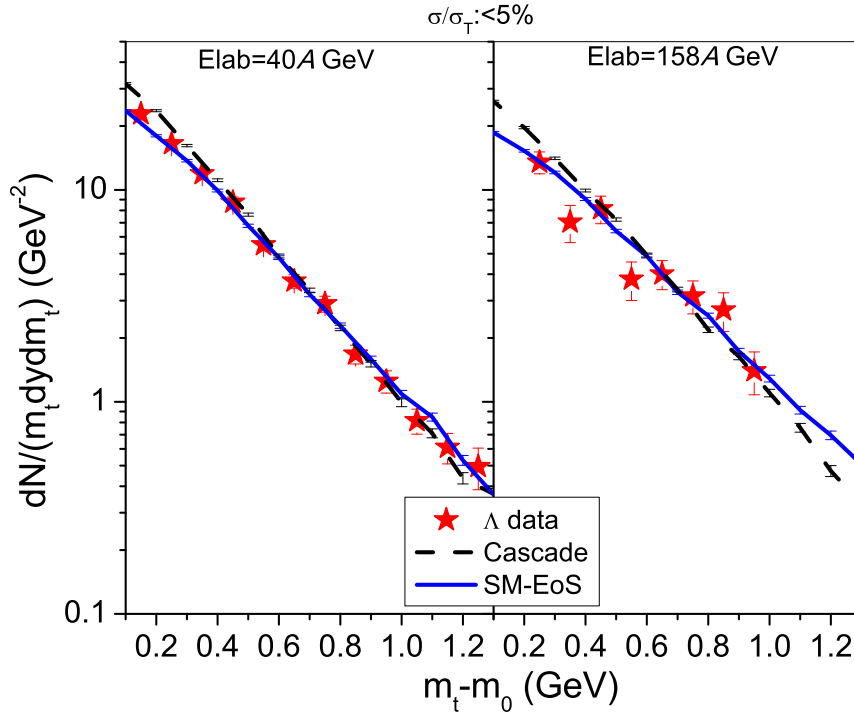


FIG. 2: Transverse mass spectra of Λs ($= \Lambda + \Sigma^0$) at mid-rapidity ($|y| < 0.4$) for central Pb+Pb reactions ($\sigma/\sigma_T < 5\%$) at 40A GeV (left plot) and at 158A GeV (right plot). The experimental data are shown by stars (taken from Ref. [34]) while calculations with mean-field potentials (dashed lines) are compared with those with a cascade mode (solid lines).

both formed and pre-formed hadron mean-field potentials, it is found that the slope becomes more flat so that one can further describe the data at both the low and the high transverse masses. Therefore, the treatment of the mean field contributions is also of importance.

Fig. 3 depicts centrality dependence of the rapidity distribution of Λ yields for Pb+Pb collisions at 40A GeV (upper plots) and 158A GeV (lower plots). Results within five centrality bins from central ($\sigma/\sigma_T < 5\%$) to semi-peripheral ($33.5\% < \sigma/\sigma_T < 43.5\%$) collisions are shown from the right to the left. First of all, it is seen that the effect of potentials is stronger in more central collisions, which is clear. Second, the potential effect is mainly to suppress the yield of hyperons at mid-rapidity which was also seen in previous calculations at lower beam energies [30]. It implies again that the dynamic transport of the hyperon after its production is important. Third, the suppression effect on the yield of hyperons provides us with a better fit to data especially at the most central collisions. We also find that calculations

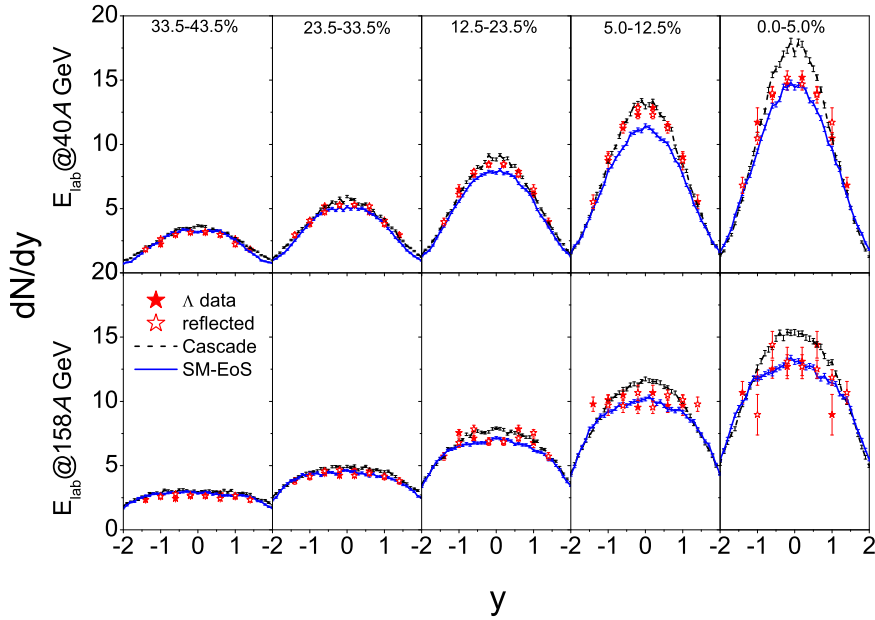


FIG. 3: Rapidity spectra of Λ s for Pb+Pb collisions at 40A GeV (upper plots) and 158A GeV (lower plots) for 5 different centrality bins which are shown from the right to the left. The experimental data in each plot is shown by stars and taken from [34]. Calculations with mean-field potentials and with a pure cascade mode are shown by lines.

with the version 2.3 also present similar results to the ones with potentials. Finally, it is also seen that in the most central Pb+Pb collisions at 158A GeV, the rapidity distribution of Λ yields calculated with potentials is slightly expanded. This phenomenon should be related to the stronger early pressure introduced by the pre-formed hadron potentials and will be discussed later-on.

Fig. 4 shows the rapidity spectra of $\bar{\Lambda}s$ ($= \bar{\Lambda} + \bar{\Sigma}^0$) for central Pb+Pb collisions at 40A GeV (left) and 158A GeV (right). Calculations with and without mean-field hadron potentials are compared to the data taken from [34]. Contrary to the rapidity distribution of Λ s, it is interesting to see that the yield of $\bar{\Lambda}s$ at mid-rapidity is driven up to fit the data quite well when the potentials are considered in calculations.

In order to understand the nice fitting results of both Λ and $\bar{\Lambda}$ spectra in both longitudinal rapidity spectra and transverse mass spectra, and to check the fitting results of other particles, we show in Fig. 5 the rapidity spectra of Ξ^- s (left) and anti-protons (right). The

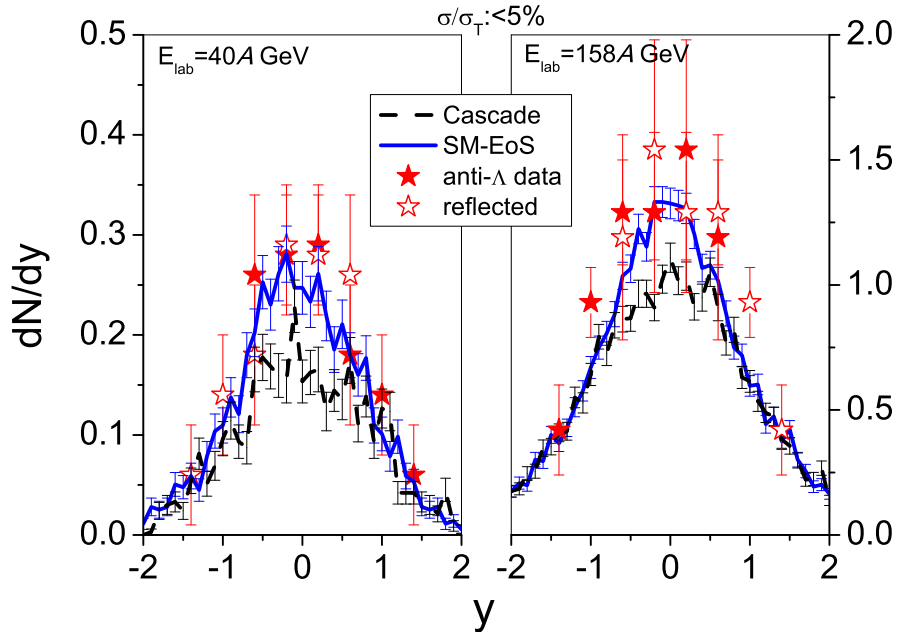


FIG. 4: Rapidity spectra of $\bar{\Lambda}$ s for central Pb+Pb collisions at 40A GeV (left) and 158A GeV (right). Experimental data and the data reflected at mid-rapidity are shown by solid and open stars [34]. Calculations with and without the mean-field potential are shown by lines.

central Pb+Pb collision at 40A GeV is chosen as an example since the experimental data are available for both particles. It is seen clearly from Fig. 5 that the calculated Ξ^- yield is suppressed with the consideration of potentials, which is the same as Λ s. While the calculated yield of anti-protons is enhanced which is the same as anti- Λ s. At 158A GeV, the same potential effect is seen for both particles.

Therefore, it is necessary to check the time evolution of these produced particles in order to understand the potential effects on both hyperons and anti-particles. Fig. 6 exhibits the calculated transverse mass spectra of Ξ^- s (left) and anti-protons (right) at two evolution time points $t = 3 \text{ fm}/c$ and $30 \text{ fm}/c$. The central Pb+Pb reaction at the beam energy 158A GeV is chosen in order to have more particles during the time evolution. From Fig. 6, we find that shortly after the time when the two Lorentz-contracted nuclei have passed through each other [48] (e.g., $\sim 3 \text{ fm}/c$ and $\sim 1.5 \text{ fm}/c$ for the Pb+Pb system at 40A GeV and 158A GeV, respectively), here we set $t = 3 \text{ fm}/c$, the potential effect on Ξ^- production can be seen at high transverse mass, but it is more obvious in the anti-proton spectra. It should be due

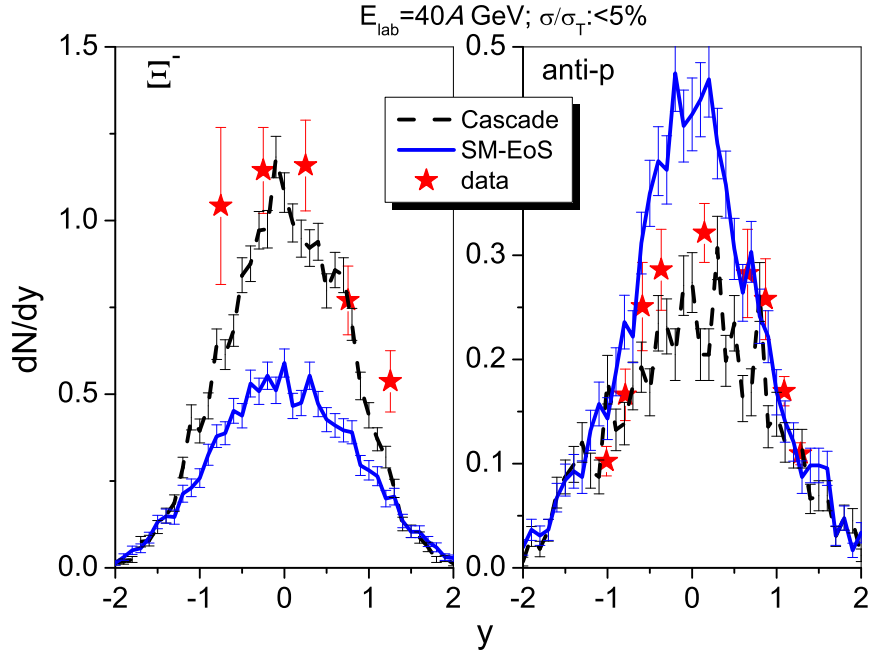


FIG. 5: Rapidity spectra of Ξ^- s (left) and anti-protons (right) for central Pb+Pb collisions at 40A GeV. Experimental data are shown by stars [31–33]. Calculations with and without the mean-field potential are shown by lines.

to the fact that anti-particles are mainly produced at earlier collisions within a more dense region. Therefore, a higher early pressure introduced by the pre-formed hadron potential leads to stronger emission of anti-protons with high momenta. With the increasing time from $t = 3 \text{ fm}/c$ to $t = 30 \text{ fm}/c$ (when most of rescatterings of particles have ceased), we find that in the cascade mode there are still a large amount of new Ξ^- s produced, while the production of anti-protons in this period becomes much less important. The time evolution of total yields of particles can be seen more clearly from Fig. 7: in the cascade mode and with the time increasing from $3 \text{ fm}/c$ to $30 \text{ fm}/c$, the total yield of Ξ^- is doubled increased, while the yield of anti-protons is about 30% decreased due to the well-known strong annihilation effect. It is also found that after $12 \text{ fm}/c$ the yield of anti-protons is almost saturated. With the consideration of formed and pre-formed hadron potentials, however, more anti-protons are survived which are mainly due to their higher momenta obtained at the early stage of reactions. If we switch off the pre-formed hadron potentials but keep the formed ones, it is seen from Fig. 7 that the time evolution of anti-protons is almost the same as that with the cascade mode. It implies that the mechanism of string excitation and fragmentation is

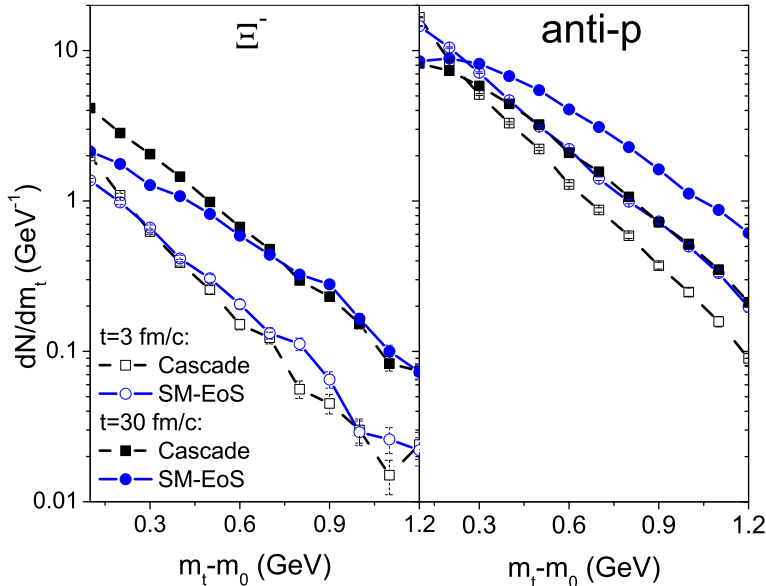


FIG. 6: Calculated transverse mass spectra of Ξ^- s (left) and anti-protons (right) for central Pb+Pb collisions at 158A GeV and at two time points: 3 fm/c and 30 fm/c. Calculation results with and without the mean-field potential are shown by lines with symbols.

essential to the production of anti-protons, which certainly is reasonable. For strange particle production, in addition to the string mechanism, the rescattering process of hadrons are also of importance, which can be understood clearly from the following features shown in Figs. 6 and 7: (1) the rapid increase of the Ξ^- yield during the time 3–30 fm/c, (2) the suppression effect of potentials on both the yield mainly at the low transverse masses shown in Fig. 6 and the total yield shown in Fig. 7 at $t = 30$ fm/c, and (3) the contribution of formed hadron potentials to Ξ^- yield (the line with half-open circle in Fig. 7).

Thus, up to now, we have understood more deeply the reason why the mean-field potentials contribute to the nice fitting results of both Λ and $\bar{\Lambda}$ spectra shown in Figs. 2-4. However, it is also found from Figs. 5-7 that the modification of the UrQMD model should carry on with more endeavors. First, the production of multi-strange baryons is still not satisfactory. The yield at mid-rapidity is underestimated at SPS energies in all versions of UrQMD calculations (including the newest version 2.3). This problem can not be solved solely by the change of the double strange diquark suppression factor and/or the single strange diquark suppression factor. Since the strange-hadron related cross sections are nor-

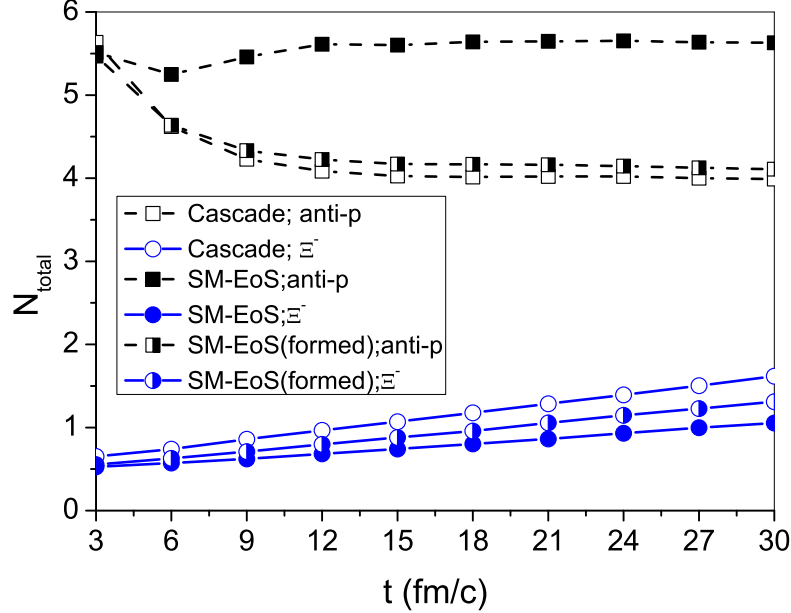


FIG. 7: Time evolution of total yields of Ξ^- s and anti-protons for central Pb+Pb collisions at 158A GeV. Cascade calculation results (line with open symbols) are compared to the results with potentials of both formed and pre-formed particles (lines with solid symbols), and to the results with potentials of only formed particles (lines with half-open symbols).

mally large, the medium effect of cross sections on the production and the rescattering of multi-strange baryons should show importance and deserves more investigations. Second, the production of (anti-) protons at AGS and SPS energies are still an open problem [31, 40]. Although the net-proton yield and the rapidity distributions of (anti-)protons are better described [36, 40] by the mean-field potential version, a further refinement is still required. The dynamic process of particles in the dense medium induced by both the new (QGP) phase and the hadronic phase afterwards should be investigated with a theoretical breakthrough.

To summarize, the production of strange baryons, especially the Λ s and $\bar{\Lambda}$ s, are investigated with the mean-field potential version of the UrQMD model for HICs at SPS energies. In this version of UrQMD, in addition to the formed hadrons, the mean-field potentials of pre-formed hadrons are also considered which are similar to those of formed hadrons. It is found that with the consideration of potentials, the transverse mass and longitudinal rapidity distributions of experimental data of both Λ s and $\bar{\Lambda}$ s can be quantitatively explained

fairly well. The early strongly repulsive and the later-on attractive forces introduced mainly by the pre-formed and the formed potentials respectively lead to more $\bar{\Lambda}$ emission but less Λ emission at freeze-out. Our investigation also shows that the hadronic rescattering process is still important for HICs at SPS energies.

Acknowledgements

We would like to thank C. Blume for sending us the experimental data and M. Bleicher for useful discussions. We acknowledge support by the computing server C3S2 in Huzhou Teachers College. The work is supported in part by the key project of the Ministry of Education of China (No. 209053), the National Natural Science Foundation of China (Nos. 10905021,10979023), the Zhejiang Provincial Natural Science Foundation of China (No. Y6090210), and the Qian-Jiang Talents Project of Zhejiang Province (No. 2010R10102).

-
- [1] H. Stoecker and W. Greiner, Phys. Rept. **137**, 277 (1986).
 - [2] J. Aichelin, Phys. Rept. **202**, 233 (1991).
 - [3] W. Cassing and E. L. Bratkovskaya, Phys. Rept. **308**, 65 (1999).
 - [4] V. Baran, M. Colonna, V. Greco and M. Di Toro, Phys. Rept. **410**, 335 (2005).
 - [5] H. Stoecker, M. Gyulassy and J. Boguta, Phys. Lett. B **103**, 269 (1981).
 - [6] C. Ko, Phys. Lett. B **120**, 294 (1983).
 - [7] I. Bombaci and U. Lombardo, Phys. Rev. C **44**, 1892 (1991).
 - [8] B. A. Brown, Phys. Rev. Lett. **85**, 5296 (2000).
 - [9] P. Danielewicz, R. Lacey and W. G. Lynch, Science **298**, 1592 (2002)
 - [10] Q. Li, Z. Li, S. Soff, M. Bleicher and H. Stoecker, Phys. Rev. C **72**, 034613 (2005)
 - [11] M. B. Tsang, Y. Zhang, P. Danielewicz, M. Famiano, Z. Li, W. G. Lynch and A. W. Steiner, Phys. Rev. Lett. **102**, 122701 (2009).
 - [12] D. H. Rischke, Y. Pursun and J. A. Maruhn, Nucl. Phys. A **595** (1995) 383 [Erratum-ibid. A **596** (1996) 717].
 - [13] C. Spieles, H. Stöcker and C. Greiner, Phys. Rev. C **57** (1998) 908.
 - [14] M. Bluhm, B. Kampfer, R. Schulze, D. Seipt and U. Heinz, Phys. Rev. C **76** (2007) 034901.

- [15] Q. Li, J. Steinheimer, H. Petersen, M. Bleicher and H. Stoecker, Phys. Lett. B **674**, 111 (2009).
- [16] W. Cassing and E. L. Bratkovskaya, arXiv:1004.3064 [nucl-th].
- [17] T. Matsui and H. Satz, Phys. Lett. B **178**, 416 (1986).
- [18] S. Soff, S. A. Bass, M. Bleicher, L. Bravina, E. Zabrodin, H. Stöcker and W. Greiner, Phys. Lett. B **471**, 89 (1999).
- [19] A. Dumitru and R. D. Pisarski, Phys. Lett. B **525**, 95 (2002).
- [20] E. Wang and X. N. Wang, Phys. Rev. Lett. **87**, 142301 (2001).
- [21] U. Heinz and G. Kestin, PoS C **POD2006**, 038 (2006).
- [22] G. Torrieri, Phys. Rev. C **76**, 024903 (2007).
- [23] S. A. Bass *et al.*, [UrQMD-Collaboration], Prog. Part. Nucl. Phys. **41**, 255 (1998).
- [24] M. Bleicher *et al.*, [UrQMD-Collaboration], J. Phys. G: Nucl. Part. Phys. **25**, 1859 (1999).
- [25] E. L. Bratkovskaya *et al.*, Phys. Rev. C **69**, 054907 (2004).
- [26] X. Zhu, M. Bleicher and H. Stoecker, Phys. Rev. C **72**, 064911 (2005).
- [27] H. Sorge, H. Stoecker and W. Greiner, Annals Phys. **192**, 266 (1989).
- [28] W. Cassing, Nucl. Phys. A **795**, 70 (2007).
- [29] Z. W. Lin, C. M. Ko and S. Pal, Phys. Rev. Lett. **89**, 152301 (2002).
- [30] Q. Li, Z. Li, E. Zhao and R. K. Gupta, Phys. Rev. C **71**, 054907 (2005).
- [31] H. Petersen, M. Bleicher, S. A. Bass and H. Stoecker, arXiv:0805.0567 [hep-ph].
- [32] M. K. Mitrovski *et al.* [NA49 Collaboration], J. Phys. G **32**, S43 (2006).
- [33] C. Blume [Na49 Collaboration], J. Phys. G **34**, S951 (2007).
- [34] T. Anticic *et al.* [NA49 Collaboration], Phys. Rev. C **80**, 034906 (2009).
- [35] Q. Li, Z. Li, S. Soff, M. Bleicher and H. Stoecker, J. Phys. G **32**, 151 (2006).
- [36] Q. Li, M. Bleicher and H. Stoecker, Phys. Lett. B **659**, 525 (2008).
- [37] J. Aichelin and H. Stoecker, Phys. Lett. B **176**, 14 (1986).
- [38] H. Petersen, Q. Li, X. Zhu and M. Bleicher, Phys. Rev. C **74**, 064908 (2006).
- [39] W. Trautmann *et al.*, Prog. Part. Nucl. Phys. **62**, 425 (2009).
- [40] Y. Yuan, Q. Li, Z. Li and F. H. Liu, Phys. Rev. C **81**, 034913 (2010) [Erratum-ibid. C **81**, 069901 (2010)].
- [41] M. Bleicher and H. Stoecker, Phys. Lett. B **526** (2002) 309.
- [42] M. A. Lisa, S. Pratt, R. Soltz and U. Wiedemann, Ann. Rev. Nucl. Part. Sci. **55** (2005) 357.
- [43] H. Petersen, J. Steinheimer, G. Burau, M. Bleicher and H. Stöcker, Phys. Rev. C **78** (2008)

044901.

- [44] T. Sjostrand, S. Mrenna and P. Z. Skands, JHEP **0605**, 026 (2006).
- [45] M. Isse, A. Ohnishi, N. Otuka, P. K. Sahu and Y. Nara, Phys. Rev. C **72**, 064908 (2005).
- [46] T. Maruyama, K. Niita, T. Maruyama, S. Chiba, Y. Nakahara and A. Iwamoto, Prog. Theor. Phys. **96**, 263 (1996).
- [47] Q. Li, M. Bleicher and H. Stocker, Phys. Lett. B **663**, 395 (2008).
- [48] J. Steinheimer, M. Bleicher, H. Petersen, S. Schramm, H. Stocker and D. Zschesche, Phys. Rev. C **77**, 034901 (2008).